

Effect of silver sulfide decorating on structural, optical and photo catalytic properties of iron-doped titanium dioxide nanotubes films

Yousef Ghayeb¹ · Mohamad Mohsen Momeni¹ · Aliakbar Mozafari¹

Received: 5 June 2016 / Accepted: 6 July 2016 / Published online: 11 July 2016
© Springer Science+Business Media New York 2016

Abstract Iron-doped titanium dioxide nanotubes (FeTiO₂ NTs) decorated with Ag₂S with good photo catalytic performance were prepared by anodization and successive ionic layer adsorption and reaction (SILAR) methods. The morphology, crystal structure, elemental composition and light absorption capability of prepared samples were characterized by FE-SEM, XRD, EDX and UV–Vis methods. SEM results show that prepared FeTiO₂ NTs have tube diameter in the range of 50–90 nm. Characterization of the Ag₂S/FeTiO₂ NTs samples indicated that Ag₂S was deposited on the surface of FeTiO₂ NTs nanotubes and also the number of SILAR cycles significantly influenced the morphology of prepared samples. The effect of the SILAR cycles on the optical and photo catalytic properties of the hybrids were studied. Results showed that the photo catalytic activity of Ag₂S/FeTiO₂ NTs samples is higher than bare FeTiO₂ NTs sample. The high photo catalytic activity of the hybrids were mainly ascribed to the narrow band gap, large specific surface area and effective heterojunction. The photo catalytic activity increase with the proper increase of Ag₂S amount; however, the activity decreases when the amount of Ag₂S is further increased which may result in the formation of the compact films on the surface and a decrease in surface area of samples. Ag₂S/FeTiO₂ NTs is easy to be recycled and has good stability for repeated use. A mechanism is also studied and an electron transfer route is provided and accounts for the enhanced photo catalytic activity. With the improved

visible light degradation performance, Ag₂S/FeTiO₂ NTs samples would be expected to be used in water purification.

1 Introduction

Titanium dioxide, as an effective photo catalyst, has been intensively investigated since Fujishima and Honda discovered the photo catalytic water splitting on TiO₂ electrodes in 1972 [1, 2]. TiO₂ has been shown to be an excellent photo catalyst due to its long-term stability, non-toxicity, low-cost preparation and a strong oxidizing power useful for the decomposition of unwanted organic compounds for the treatment of waste water and air pollution. However, this material is only active under UV excitation because of its large energy band gap of 3.2 eV (in its anatase form). Considering that the fraction of UV light is less than 5 % in the total solar spectrum on the earth, it is crucial and a great challenge to develop efficient, visible light-active photo catalysts [3–8]. Thus, band gap engineering of photo catalysts to induce absorption into the wide visible light region has been considered as a possible solution to this problem. Doping nitrogen, sulfur and some metal cations were usually used to narrow the band gap of TiO₂ [9–13]. The iron doping has been reported to be effective in enhancing photo catalytic activity and mineralization of TiO₂ and more effective than other metal cations [12–17]. The effect of iron doping can be ascribed to the band gap narrowing of TiO₂ and/or photo-generated electrons/holes from Fe impurity energy levels [18–20]. To further enhance the photo catalytic property, various heterojunction nanostructures of two and three semiconductors, which can promote effective separation between photo-generated electrons and holes, are widely attended. Silver sulfide (Ag₂S), owing to its narrow band gap

✉ Yousef Ghayeb
ghayeb@cc.iut.ac.ir

¹ Department of Chemistry, Isfahan University of Technology, Isfahan 84156-83111, Iran

($E_g \sim 1.0$ eV) and relatively high absorption coefficient of visible light, is considered to be an important binary compound semiconductor [21, 22]. Hence, Ag_2S is a highly desirable material that can be used in photovoltaics and photo-electrochemistry [23–26]. It is a promising material which responds in the whole solar energy spectrum. Although there were some reports about the coupling of TiO_2 with Ag_2S semiconductor, rarely studies regarding FeTiO_2 NTs and Ag_2S were conducted [27, 28].

In the present study, we reported an effective synthetic strategy for preparation of iron-doped titanium dioxide nanotubes (FeTiO_2 NTs) decorated with Ag_2S with excellent photo catalytic performance. Doping TiO_2 NTs with iron is an effective approach to reduce electron–hole recombination rate and increase photo catalytic efficiency in terms of its semi-full electronic configuration and ion radius close to Ti^{4+} . FeTiO_2 NTs were prepared by the electrochemical anodic oxidation of pure titanium, followed by annealing treatment. Subsequently, Ag_2S was deposited on the as-prepared samples by successive ionic layer adsorption and reaction (SILAR) methods. The morphology and structure were characterized by scanning electron microscopy, energy dispersive X-ray spectroscopy and X-ray diffraction. Optical properties were investigated by UV–visible diffuse reflectance spectra. In addition, photo catalytic activity of different hybrid nanostructure samples were investigated and compared by degradation of methylene blue (MB). To the best of our knowledge, till now, very less research has been done to preparing of $\text{Ag}_2\text{S}/\text{FeTiO}_2$ NTs samples by anodizing and SILAR process.

2 Experimental

All chemicals were obtained as analytical reagent grade and used without further purification. The solutions were prepared with distilled water. Titanium foils (purity >99.99 %, 1 mm thickness) were used.

FeTiO_2 NTs were synthesized by in situ anodizing of titanium in a solution of ethylene glycol (98 mL) containing 0.13 M NH_4F and 2 mL distilled water, followed by the dissolution 9 mM of potassium ferricyanide [$\text{K}_3\text{Fe}(\text{CN})_6$]. Before the anodizing, the titanium electrode was mechanically polished with different emery type abrasive papers (with the following grades: 80, 180, 400, 600, 1200 and 2000), rinsed in a bath of distilled water, and then chemically etched by immersing in a $\text{HF}/\text{HNO}_3/\text{H}_2\text{O}$ (1:4:5 in volume) mixed solution. The last step of pretreatment was rinsing with distilled water. The anodizing experiments were carried out using a two-electrode system with titanium foil as anode and graphite foil with about 12 cm^2 geometric areas as cathode, respectively. Anodizing was carried out under a constant voltage of 60 V for 6 h at room temperature. After

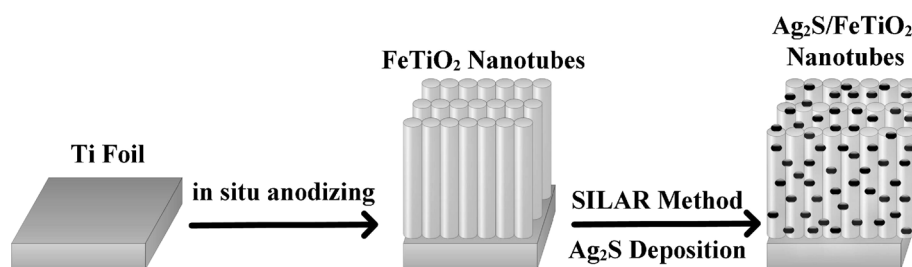
anodizing, the as-formed samples were annealed in air atmosphere at 400 °C for 2 h with a ramp of 2 °C/min to obtain crystalline samples. Then silver sulfide (Ag_2S) was decorated on the FeTiO_2 NTs by separately SILAR method. FeTiO_2 NTs were dipped into 0.1 M AgNO_3 in ethanol for 1 min, rinsed with ethanol and dipped for 3 min in a 0.1 M Na_2S methanol solution and rinsed again with ethanol, which was defined as one SILAR cycle. The deposition of Ag_2S was repeated for 8 cycles. In order to investigate the influence of deposition conditions on samples property, we changed the deposition cycle (0, 2, 3, 4, 5, 6 and 8 cycles) into carry out the $\text{Ag}_2\text{S}/\text{FeTiO}_2$ NTs samples. The as prepared samples were named respectively S0, S2, S3, S4, S5, S6 and S8, that terminal number is the number of SILAR cycles. A schematic representation of the anodizing setup and producing process of FeTiO_2 NTs films on titanium and deposition of Ag_2S on these films by SILAR method is presented in Fig. 1.

The surface morphology of all samples were characterized by field emission scanning electron microscopy (FE-SEM, Hitachi S-4160, Japan), and the elemental composition was estimated by energy dispersive X-ray spectroscopy (EDX). Elemental mapping was conducted by energy dispersive spectroscopy (EDS). The crystalline phases were identified by XRD (Philips X'Pert). Diffraction patterns were recorded in the 2θ range from 20° to 80° at room temperature. The optical absorption of the samples were determined using a diffuse reflectance UV–visible spectrophotometer (JASCO V-570). Photo catalytic activities of all the samples were evaluated by degradation of the aqueous methylene blue (MB) under visible light irradiation. The photo catalytic reaction was carried in a single-compartment cylindrical quartz reactor. A 200 W xenon lamp accompanied with a UV cutoff filter, to eliminate the radiations below wavelength of 420 nm, was used as a light source to provide visible light. The luminous intensity of the xenon lamp was $100\text{ mW}/\text{cm}^2$. The actual experiments were performed at room temperature. The initial concentration of methylene blue was 5 mg/L. Prior to illumination, the photo catalyst sample was immersed in quartz reactor containing methylene blue and magnetically stirred for 1 h in the dark to ensure the establishment of an adsorption–desorption equilibrium between the photo catalyst and methylene blue. Then the solution was exposed to visible light irradiation under magnetic stirring for 1 h. At certain time intervals, specific amount of the solution was withdrawn and the changes in concentration of MB were observed using a UV–Vis spectrophotometer.

3 Results and discussion

Iron-doped titanium dioxide nanotubes (FeTiO_2 NTs) were prepared by in situ electrochemical anodizing method. The in situ electrochemical anodizing method is a simple

Fig. 1 Schematic presentation of producing process of FeTiO₂ NTs on titanium foils and deposition of Ag₂S on these films by SILAR method



method for synthesized composite titanium dioxide nanotubes. Formation mechanism of FeTiO₂ NTs on the surface titanium in this work includes the following steps:

Oxidation of the metal which releases Ti⁴⁺ ions and electrons, Eq. (1):



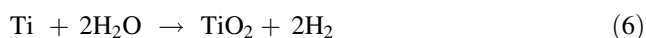
Combination of Ti⁴⁺ ions with OH⁻ and O²⁻ species provided by the water. Equations (2) and (3) below account for the hydrated anodic layer and the oxide layer. Further oxide is produced when the hydrated anodic layer releases water by a condensation reaction, Eq. (4):



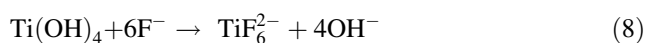
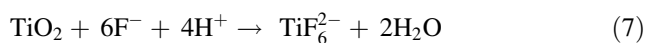
At the cathode there is hydrogen evolution, Eq. (5):



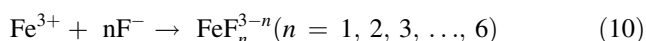
By summing the equations from (1) to (5), the overall process of oxide formation is given:



Furthermore, the fluorine ions can attack the hydrated layer and the oxide, as described in the Eqs. (7) and (8), or react with Ti⁴⁺, Eq. (9), the ions being mobile in the anodic layer, under the high applied electric field:



Clearly, the competition between formation of the oxide [see Eqs. (2)–(4)] and its dissolution [see Eqs. (7)–(9)], is the key factor in determining the anodic titanium oxide structure produced [29]. In addition to the above reactions, in electrolyte containing potassium ferricyanide (K₃Fe(CN)₆), the following reaction could be done:



Equation (10) is the coordination reaction between iron ions and fluorine ions. When potassium ferricyanide was

added to anodizing solution, the above reaction occurs between of Fe³⁺ ions and fluoride ions. As well as other reactions could be done [Eq. (11)].



There for, because (FeF_n³⁻ⁿ) and (Fe(CN)₆³⁻) com-

plexes are negatively charged, they can move to the positive terminal (anode), where electrochemical oxidation of titanium occurs, and there they can penetrate in the structure of TiO₂ nanotubes and produced iron-doped titanium dioxide nanotubes (FeTiO₂ NTs).

The SILAR technique for the deposition of thin films was introduced by Nicolau in the mid-1980s [30]. It is based on a heterogeneous reaction between adsorbed ions and solvated ions on the solid–liquid interface. The substrate is treated separately with each aqueous precursor solution so that the individual steps, adsorption and reaction, can take place. During the first step, cations are adsorbed onto the substrate, and in the next step all the excess unadsorbed cations are washed away by rinsing the substrate with purified water or ethanol. The rinsing is followed by the reaction step, during which the substrate is immersed into a vessel containing the anion precursor solution. When the solvated anions enter the diffusion layer they react with the adsorbed cations, and a solid adsorbed compound is formed on the surface. Again the ions in the diffusion layer are washed away with a rinsing pulse. By repeating these deposition steps a thin smooth film can be grown layer by layer. The thickness of the growing film is controlled by the number of deposition cycles. In SILAR method, the growth mechanism involves three most important steps:

Step I Specific adsorption of the most strongly adsorbed ions of the compound to be grown by substrate immersion in a solution of one of its salts

Step II Water or ethanol rinsing of the excess solution still adhering to the substrate

Step III Chemical reaction between the most strongly specifically adsorbed ions and the less strongly adsorbed ones by the subsequent substrate immersion in a solution containing the latter, entailing the growth [30].

The SILAR method resembles CBD but deposition control of the growth is easier since the precursors for the cation and anion constituents of the thin film are in different vessels. The growth of thin films in the SILAR method occurs only heterogeneously on the solid-solution interface due to the intermediate rinsing step between the cation and anion immersions. Therefore, the thickness of the film can be controlled simply by the number of growth cycles. The equipment for the SILAR technique can be very simple and inexpensive due to the ambient growth conditions used. The SILAR process is analogous with the atomic layer deposition ALD process where deposition is carried out in the gas phase at elevated temperature and reduced pressure.

The morphology of prepared samples were observed by SEM. Figure 2a shows FE-SEM images of FeTiO₂ NTs films on titanium which clearly shows formation of films containing vertically ordered nanotube arrays that the surface of them was open. Diameter of these FeTiO₂ tubes is in the range of 50–90 nm and their wall thickness is 50–80 nm. In cross-sectional view of FeTiO₂ sample, it can be seen that the nanotubes are parallel aligned and are very

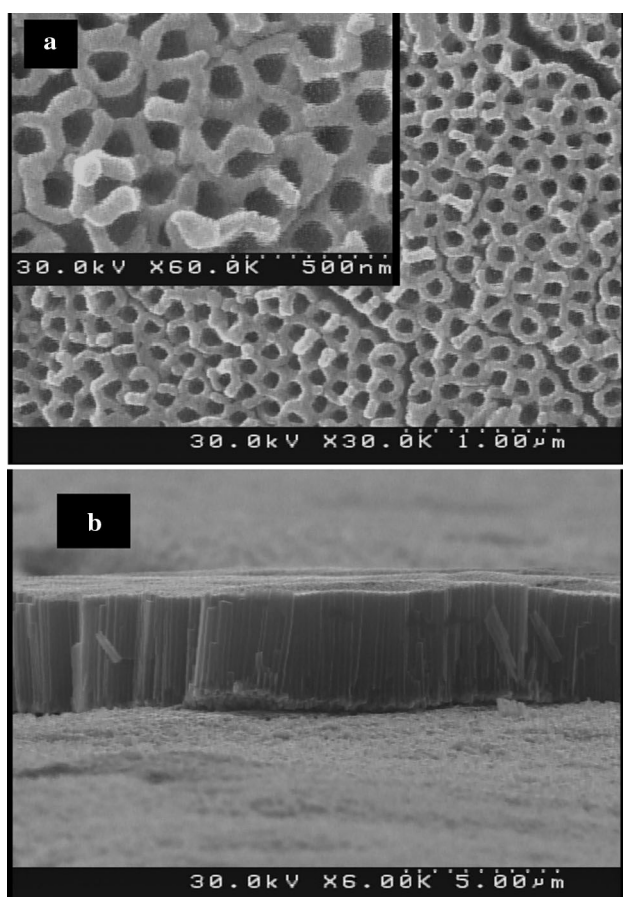


Fig. 2 **a** SEM top-view image of as-prepared FeNTs nanotubes and **b** cross-sectional images of this sample

regular. The tubes are well separated and there is distinct and clear boundary between them. The FE-SEM of different Ag₂S/FeTiO₂ NTs samples were illustrated in Fig. 3. In Fig. 3a–c, sample displayed nanotube that deposits of Ag₂S present on the surface of S2, S3 and S4 sample. Figure 3d–f showed the morphologies of S5, S6 and S8 samples, respectively. Here the entire surface is covered by Ag₂S and the greater amount of Ag₂S was deposited on the surface of these samples. In these figures, non-uniform porous films can be seen on the surface of samples. By increasing the cycle number of SILAR, more amounts of silver sulfide have been deposited on the surface. In these figures, nanostructures (nanotubes or nanoporous) can not be seen on the surface. It can be said that when the number of SILAR cycles increased to 3 cycles, surface is covered with a porous layer of Ag₂S.

The analysis of the films surface by energy dispersive X-ray spectroscopy (EDX) taking measurements on top and results present in Fig. 4. It was seen that the films mainly consisted of Ti, Fe, O, Ag and S; the contents of each sample were inserted in the corresponding figure. The EDX data of Ag₂S/FeTiO₂ NTs samples show two peaks around 4.5 and 4.9 keV for Ti. The peaks due to iron are clearly distinct at 0.5, 0.6 and 6.4 keV. The peaks due to silver are clearly distinct at 2.9 and 3.1 keV. Also peaks due to sulfur were appeared at 0.1 and 2.3 keV. These results confirm that Ti, Fe, O, Ag and S exist in these samples. The occurrences of traces of contaminants such as N and F from precursors are also observed. The composition of the Ag₂S/FeTiO₂ NTs sample was confirmed by energy-dispersive X-ray mapping (Fig. 5). This test shows the presence of Ag, S, Ti, Fe, O, Na, F and N in these samples. The elemental maps demonstrated that Ti, Fe, Ag and S are homogeneously distributed on the surface of samples.

The phase structures of samples were determined by X-ray diffraction (XRD). The XRD patterns of the bare FeTiO₂ NTs and Ag₂S/FeTiO₂ NTs samples are shown in Fig. 6. Figure 6 shows XRD patterns of (a) pure TiO₂ NTs annealed at 400 °C, (b) bare FeTiO₂ NTs annealed at 400 °C and (c) Ag₂S/FeTiO₂ NTs samples. Diffractions that are attributable to anatase TiO₂ are clearly observed in the annealed sample. The Ti peaks were due to the titanium substrate. As shown in this figure, the peaks at $2\theta = 25.3^\circ$, 37.9° , 38.6° , 48.2° and 76.2° were assigned to the TiO₂ anatase phase (JCPD card no. 01-073-1764). Four peaks at $2\theta = 30.2^\circ$, 32.1° , 56.1° and 69.3° were assigned to the Fe₂O₃ phase (JCPD card no. 00-039-1346). Comparing the XRD patterns of b and c show that apart from the existed diffraction peaks in b and c spectra which are related with the characteristic diffraction peaks of TiO₂, other specific diffraction peaks at 31.5° , 34.7° , 37.1° , 43.4° , 54.2° and 63.2° also appear in c spectrum. According to the standard

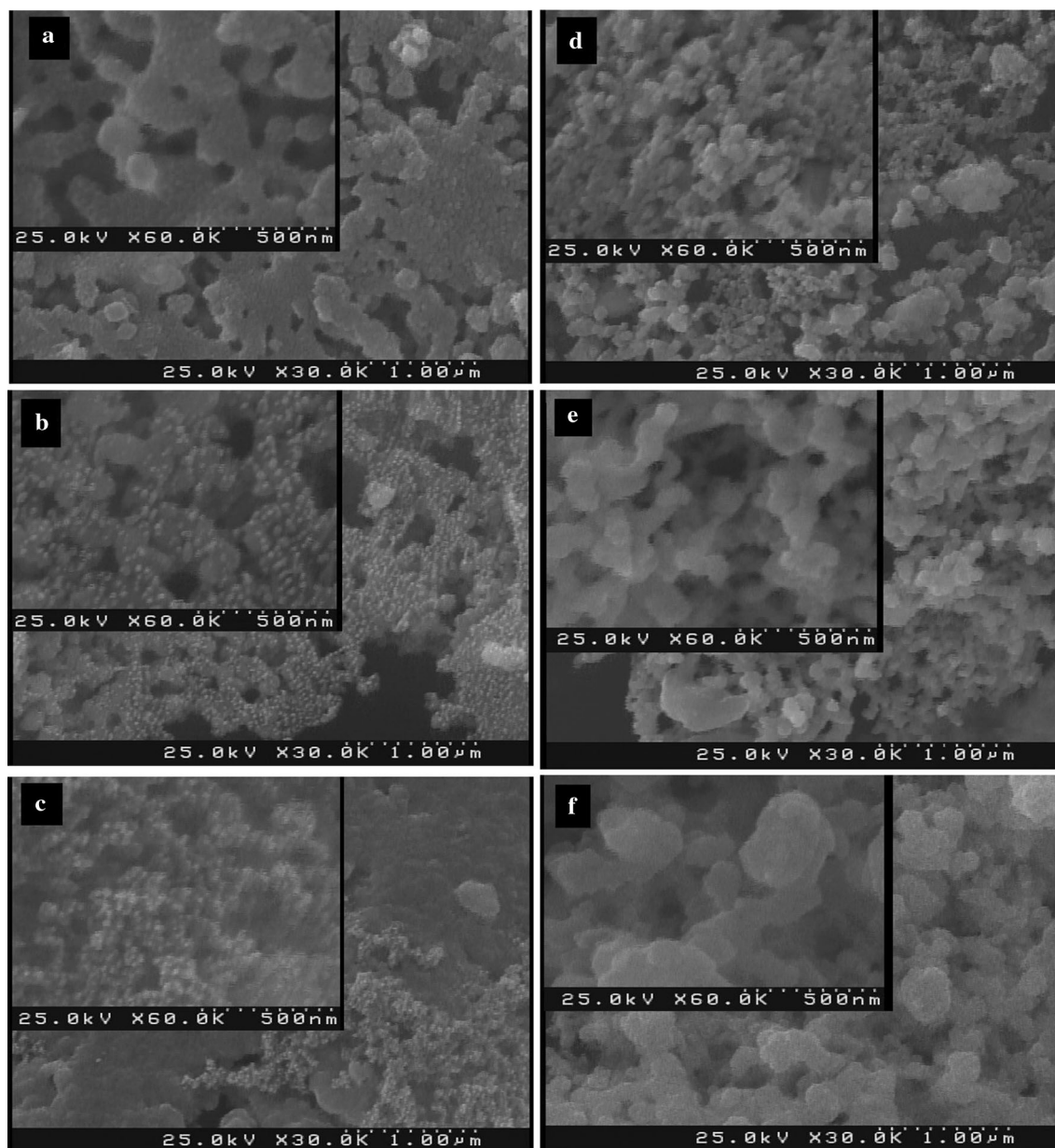


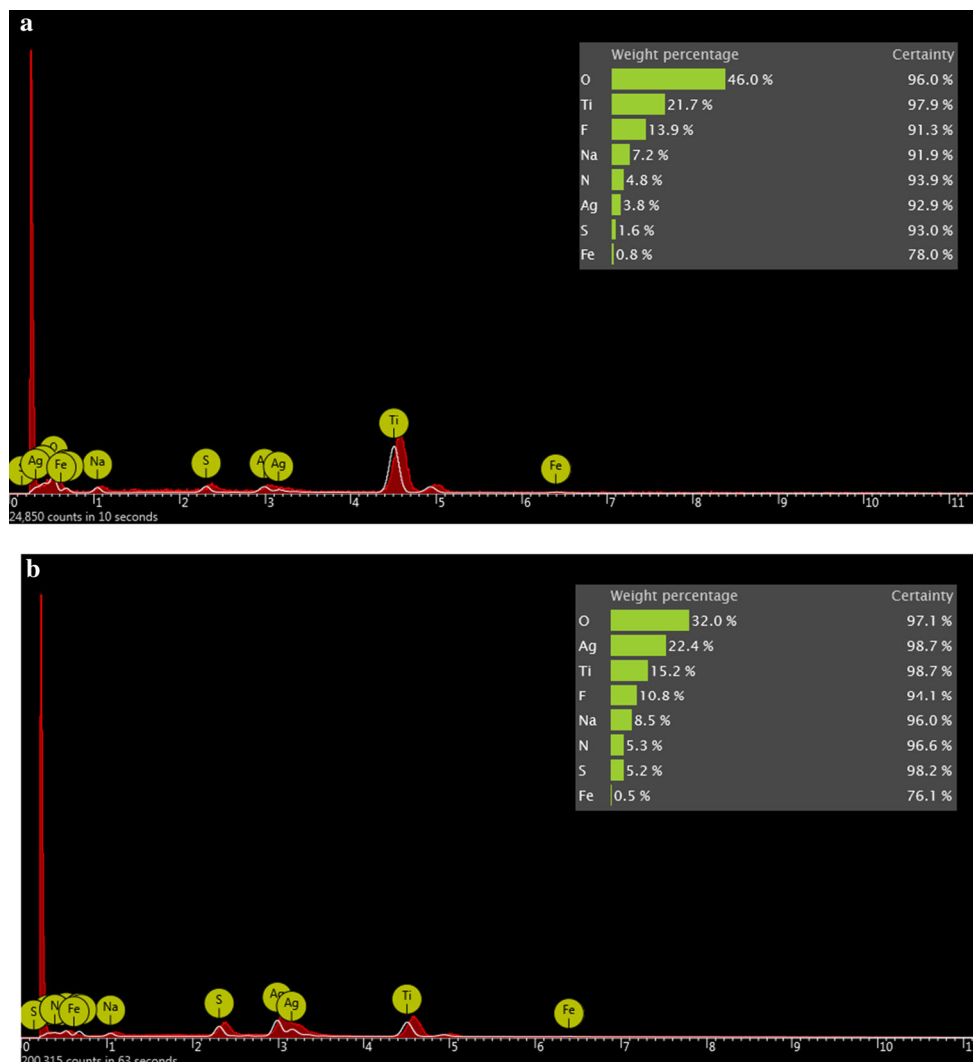
Fig. 3 SEM top-view images of different samples; **a** S2, **b** S3, **c** S4, **d** S5, **e** S6 and **f** S8

PDF (JCPD card no. 00-014-0072) of Ag_2S , the six extra specific diffraction peaks in **c** spectrum correspond with (-112) , (002) , (013) , (200) , (041) and (213) of crystal planes of Ag_2S . The diffracted intensity of six diffraction peaks is weak, which is owing to the poor crystallinity of Ag_2S without thermal treatment. The XRD data further confirms the successful preparation of $\text{Ag}_2\text{S}/\text{FeTiO}_2$ NTs samples. Also, no peaks for other impurities were found in the spectra, revealing the high purity of all products.

The light absorption properties of the pure Ag_2S , bare FeTiO_2 NTs and $\text{Ag}_2\text{S}/\text{FeTiO}_2$ NTs composites were characterized by UV–Vis diffuse reflectance spectroscopy.

As shown in Fig. 7, bare FeTiO_2 NTs sample has the absorption edge of around 300–400 nm. The broadened peaks at about 400–600 nm are similar to the reported UV–Vis spectra of pure Ag_2S . The absorption edge of $\text{Ag}_2\text{S}/\text{FeTiO}_2$ NTs composites ranges from 400 to 550 nm. The absorption edges of the composite samples shifted to longer wavelengths as the amount of Ag_2S increased. The Ag_2S with a narrow band gap display a significant growth trend with the increase of the wavelength in the range of 400–550 (Fig. 7b). The band gap energy of a semiconductor was calculated using the equation:

Fig. 4 EDX spectrum of different samples; **a** S2 and **b** S8 sample



$$\alpha h\nu = A(h\nu - E_g)^{n/2} \tag{12}$$

where α , h , ν , A and E_g are the absorption coefficient, Planck’s constant, light frequency, proportional constant and band gap, respectively. Among them, n is determined from the type of optical transition of a semiconductor. As the previous literature has reported, the n values of Ag_2S is 4. After calculating experimental data, E_g of Ag_2S was determined from a plot of $(\alpha h\nu)^2$ versus energy ($h\nu$), and the band gap energy of Ag_2S is approximately 1.1 eV (Fig. 7a), which is in good agreement with previous reports for the band gap energy of Ag_2S (0.9–1.1 eV) [31–34].

Photo catalytic activity of different samples were followed through degradation of methylene blue as a function of irradiation time with visible light. To get the response of photo catalytic activities of bare $FeTiO_2$ NTs and $Ag_2S/FeTiO_2$ NTs samples, the absorption spectra of exposed

samples at various time intervals were recorded and the rate of color degradation was observed in terms of change in intensity at λ_{max} of the dye. The degradation efficiency of samples can be estimated by the following equation:

$$\text{Degradation efficiency \%} = [(C_0 - C)/C_0] \times 100 \tag{13}$$

where C_0 and C are initial concentration of solutions and concentration of methylene blue after irradiation at various time interval, respectively.

In practice, the first, dyes degradation experiments were conducted under light irradiation to evaluate direct photolysis without the addition of any catalyst. The concentration of dyes remained nearly constant after irradiation. Thus, no obvious degradation of these dyes was observed in this time period. In addition, a dark control experiment was conducted, indicating that the adsorption of these dyes onto the surface of the catalyst in the absence of light

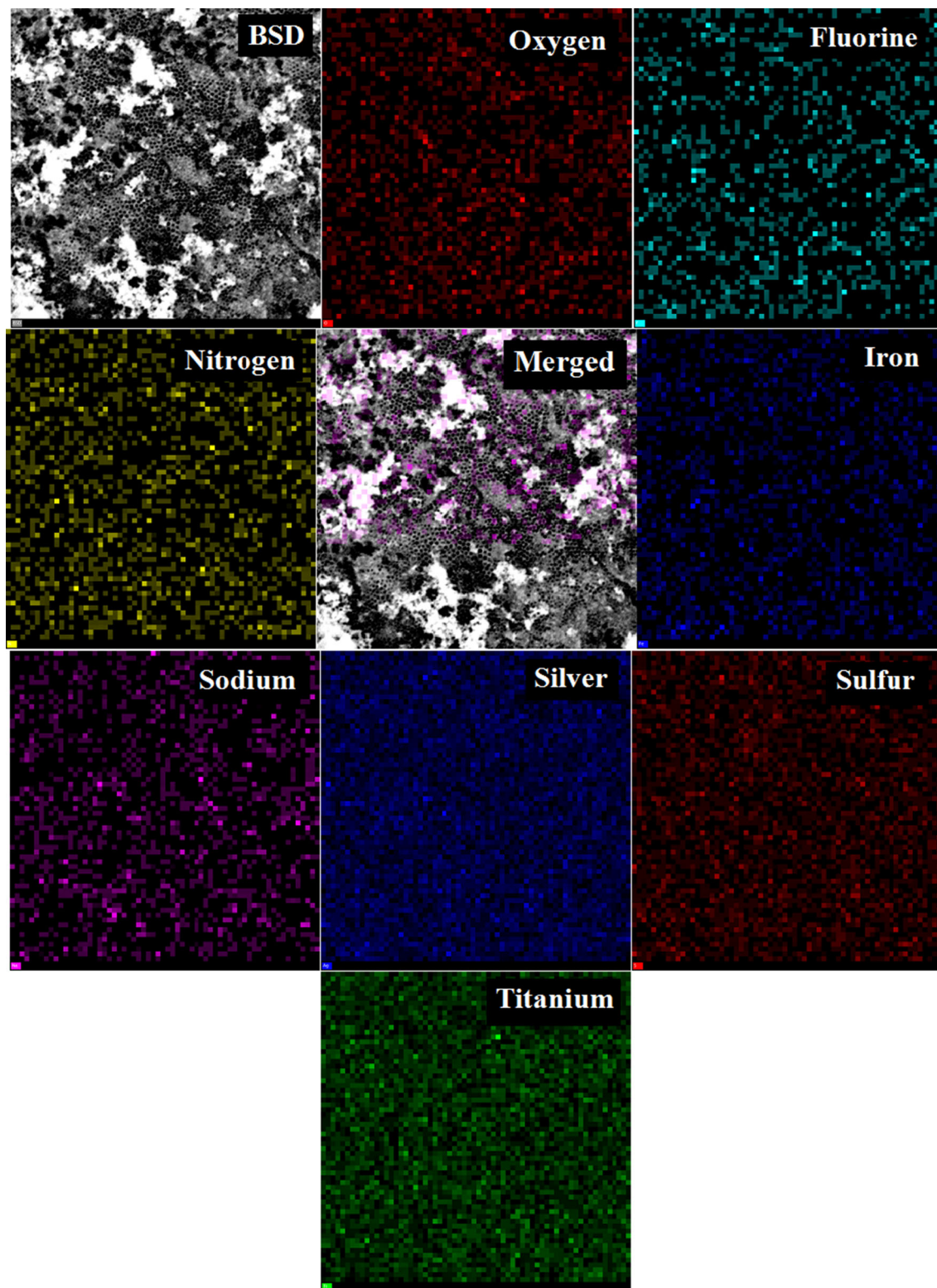


Fig. 5 Elemental EDX mapping of *Ti*, *Fe*, *O*, *Ag* and *S* obtained from S8 sample

radiation was negligible. The photo catalysis results indicated that the photo catalytic process was very effective in the removal of this dye and it was observed that the

degradation of dye was enhanced using $\text{Ag}_2\text{S}/\text{FeTiO}_2$ NTs samples. Figure 8a shows the photo-degradation rate of MB under visible light in presence of different samples.

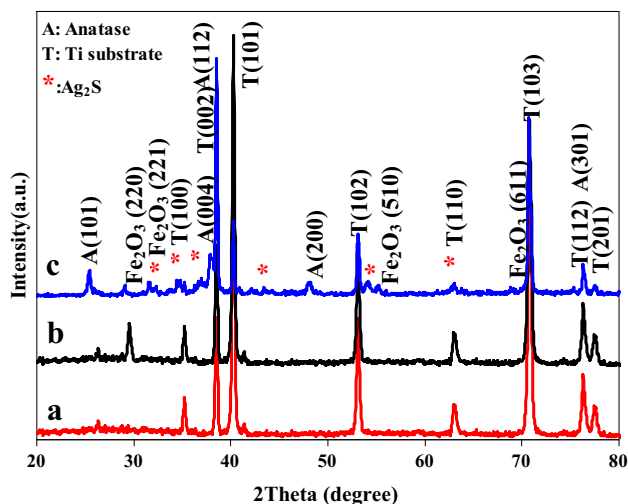


Fig. 6 XRD patterns of prepared samples *a* pure TiO₂ annealed at 400 °C for 2 h, *b* bare FeTiO₂ NTs annealed at 400 °C for 2 h and *c* S8 sample

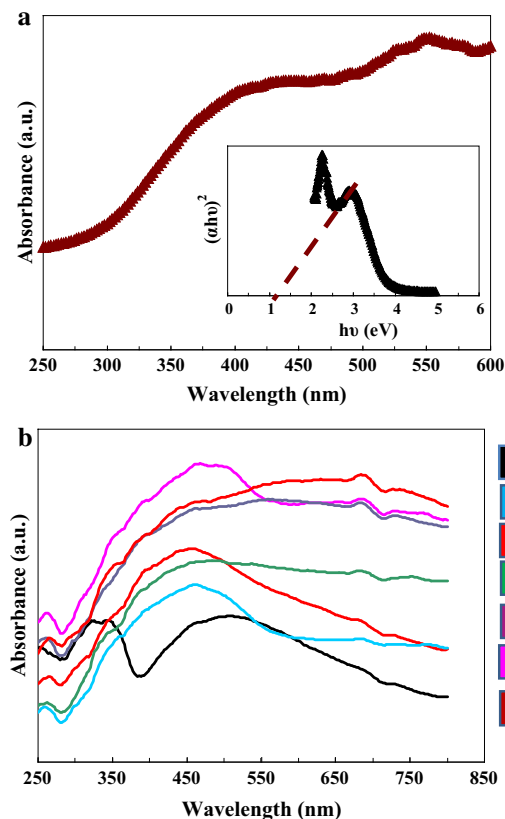


Fig. 7 *a* UV-Vis reflectance spectrum of Ag₂S sample; *Inset* $(\alpha h\nu)^2$ versus $h\nu$ for Ag₂S. *b* Diffuse reflectance UV-Vis absorption spectra of different samples

Figure 8a shows that the S3 sample exhibited better photo catalytic activity than other samples under visible light illumination. The photo catalytic performances of different samples were in the following order:

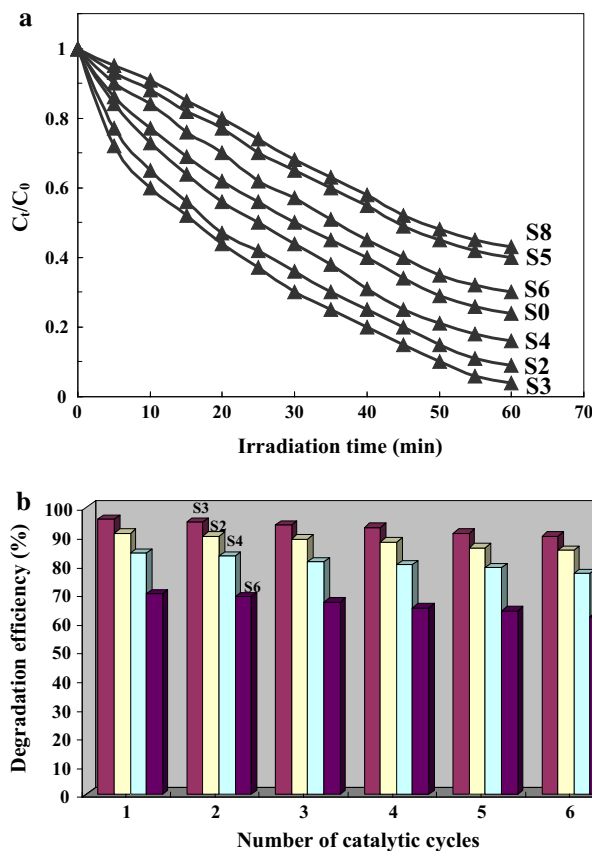


Fig. 8 *a* The photo catalytic degradation of MB over the different samples under visible light irradiation. *b* Photo catalyst stability test of prepared samples

S3 > S2 > S4 > S0 > S6 > S5 > S8

In addition to the photo catalytic activity, the stability of the photo catalysts is another important issue for practical application, for it can be regenerated and reused. To investigate the stability of prepared sample, six runs of cycling photo-degradation experiments under identical conditions were performed (Fig. 8b). Before each experiment, the used photo catalyst was cleaned through washing with distilled water. Compared with the common catalysts in the powder form that nanoparticles dispersed in the reaction media, our samples prepared on the titanium substrates are more conveniently separated and recycled without any laborious centrifugation. As shown in Fig. 8b, after a 6-cycle experiment, this catalyst exhibited similar catalytic performance without significant deactivation, indicating its high durability and stability.

Schematic diagram of energy levels and initial redox process of the Ag₂S/FeTiO₂ NTs hybrids in the process of visible light excitation can be proposed in Fig. 9. Because the energy level of absolute conduction band (E_c) of the

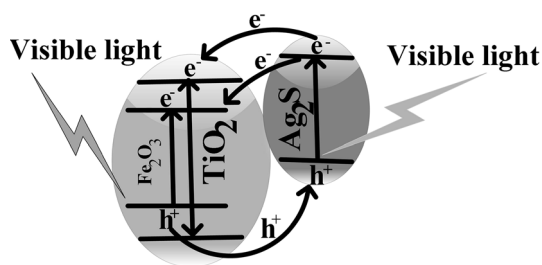


Fig. 9 Mechanism of photo catalytic degradation of MB using $\text{Ag}_2\text{S}/\text{FeTiO}_2$ NTs

Ag_2S is higher than that of Fe_2O_3 and TiO_2 , electron movement from Ag_2S to Fe_2O_3 is possible. This leads to that the electron transformation from the Ag_2S to the conduction band of Fe_2O_3 . In addition, the E_c of the Ag_2S is higher than that of TiO_2 , leading to that the electrons in the Ag_2S can transfer to the conduction band of TiO_2 . The increased number of electrons in the conduction band of Fe_2O_3 and TiO_2 , can directly reduce the dye or be used as reducing agents, producing OH^- , or resulting in the formation of reactive oxygen-based radicals, such as O^{2-} . The O^{2-} upon protonation produces hydroperoxy radicals (HO_2^-) and eventually hydroxyl radicals (OH) are formed [35, 36]. Moreover, the remained and/or increased electrons in the TiO_2 conduction band can also either directly reduce the dye or react with adsorbed water molecules and surface OH groups, producing OH^- [35–37]. The produced OH and OH^- groups play a role of oxidation and reduction in the photo-degradation process, respectively. As a result, the photo catalytic activity of the hybrids can be enhanced with increasing effective photo-generated electrons and holes as increasing Ag_2S ratio.

4 Conclusion

The major conclusions from the present work are as follows:

- Iron-doped titanium dioxide nanotubes (FeTiO_2 NTs) were successfully synthesized using a facile single-step anodizing method.
- $\text{Ag}_2\text{S}/\text{FeTiO}_2$ NTs were successfully synthesized via two methods; anodization and successive ionic layer adsorption and reaction (SILAR) method.
- These catalysts were characterized by FE-SEM, EDX, XRD and UV–Vis.
- SEM results show that prepared FeTiO_2 NTs have tube diameter of 50–90 nm
- SEM of $\text{Ag}_2\text{S}/\text{FeTiO}_2$ NTs samples show that Ag_2S deposited on the surface of nanotubes and the number

of SILAR cycles significantly influenced the morphology of prepared samples.

- XRD and EDX analysis showed presence of Fe_2O_3 and Ag_2S on prepared samples.
- The effect of the SILAR cycles on the optical and photo catalytic properties of the hybrids were studied.
- Compared with the bare FeTiO_2 NTs, $\text{Ag}_2\text{S}/\text{FeTiO}_2$ NTs exhibited enhanced photo catalytic activity in the degradation of MB under visible light illumination, which could be attributed to the narrow band gap, large specific surface area and effective heterojunction.
- $\text{Ag}_2\text{S}/\text{FeTiO}_2$ NTs is easy to be recycled and has good stability for repeated use
- The process developed in this study is facile, reproducible, and inexpensive and can be easily scaled up.

References

1. A. Fujishima, K. Honda, *Nature* **238**, 37 (1972)
2. W.J. Zhou, Y.H. Leng, D.M. Hou, H.D. Li, L.G. Li, G.Q. Li, H. Liu, S.W. Chenad, *Nanoscale* **6**, 4698 (2014)
3. M.M. Momeni, Z. Nazari, *Ceram. Int.* **42**, 8691 (2016)
4. H. Zhang, X.J. Lv, Y.M. Li, Y. Wang, J.H. Li, *ACS Nano* **1**, 380 (2010)
5. M.M. Momeni, Y. Ghayeb, *J. Mol. Catal. A Chem.* **417**, 107 (2016)
6. W.J. Zhou, G.J. Du, P.G. Hu, Y.Q. Yin, J.H. Li, J.H. Yu, G.C. Wang, J.X. Wang, H. Liu, J.Y. Wang, H. Zhang, *J. Hazard. Mater.* **197**, 19 (2011)
7. M.M. Momeni, Y. Ghayeb, *Ceram. Int.* **42**, 7014 (2016)
8. M.M. Momeni, Y. Ghayeb, *J. Solid State Electrochem.* **20**, 683 (2016)
9. T. Lindgren, J.M. Mwabora, E. Avendano, J. Jonsson, A. Hael, C. Granqvist, S. Lindqvist, *J. Phys. Chem. B* **107**, 5709 (2003)
10. K. Nishijima, B. Ohtani, X.L. Yan, T.A. Kamai, T. Chiyoya, T. Tsubota, N. Murakami, T. Ohno, *Chem. Phys.* **339**, 64 (2007)
11. T. Umebayashi, T. Yamaki, H. Itoh, K. Asai, *Appl. Phys. Lett.* **81**, 454 (2002)
12. W.Y. Choi, M. Hoffmann, *J. Phys. Chem.* **98**, 13669 (1994)
13. R.L. Narayana, M. Matheswaran, A.A. Aziz, P. Saravanan, *Desalination* **269**, 249 (2011)
14. X.X. Yang, C.D. Cao, L. Erickson, K. Hohn, R. Maghirang, K. Klabunde, *Appl. Catal. B* **91**, 657 (2009)
15. Y.R. Zhang, Q. Li, *Solid State Sci.* **16**, 16 (2013)
16. D.V. Wellia, Q.C. Xu, M.A. Sk, K.H. Lim, T.M. Lim, T. Thatt, Y. Tan, *App. Catal. A* **401**, 98 (2011)
17. P. Sathishkumar, S. Anandan, P. Maruthamuthu, T. Swaminathan, M.F. Zhou, M. Ashokkumar, *Coll. Surf. A* **375**, 231 (2011)
18. L.G. Devi, R. Kavitha, *Appl. Catal. B Environ.* **140**, 559 (2013)
19. S. Tieng, A. Kanaev, K. Chhor, *Appl. Catal. A* **399**, 191 (2011)
20. M.M. Momeni, Y. Ghayeb, *J. Mater. Sci. Mater. Electron.* **27**, 1062 (2016)
21. Y. Xie, S.H. Heo, Y.N. Kim, S.H. Yoo, S.O. Cho, *Nanotechnology* **21**, 015703 (2009)
22. K. Nagasuna, T. Akita, M. Fujishima, H. Tada, *Langmuir* **27**, 7294 (2011)

23. Y. Xie, S.H. Yoo, C. Chen, S.O. Cho, *Sci. Eng. B Adv. Funct. Solid-State Mater.* **177**, 106 (2012)
24. B. Liu, D. Wang, Y. Zhang, H. Fan, Y. Lin, T. Jiang, T. Xie, *Dalton Trans.* **42**, 2232 (2013)
25. Z.D. Meng, T. Ghosh, L. Zhu, J.G. Choi, C.Y. Park, W.C. Oh, *J. Mater. Chem.* **22**, 16127 (2012)
26. H. Hu, J. Ding, S. Zhang, Y. Li, L. Bai, N. Yuan, *Nanoscale Res. Lett.* **8**, 1 (2013)
27. M.C. Neves, O.C. Monteiro, R. Hempelmann, A.M.S. Silva, T. Trindade, *Eur. J. Inorg. Chem.* **28**, 4380 (2008)
28. Y. Xie, S.H. Heo, Y.N. Kim, S.H. Yoo, S.O. Cho, *Nanotechnology* **21**, 015703 (2010)
29. M. Hosseini, M.M. Momeni, M. Faraji, *Electroanalysis* **23**, 1654 (2011)
30. Y.F. Nicolau, *Appl. Surf. Sci.* **23**, 1061 (1985)
31. P. Ma, H. Yu, W. Wang, H. Wang, J. Zhang, Z. Fu, *Phys. Chem. Chem. Phys.* **18**, 3638 (2016)
32. W. Yang, T. Xie, D. Wang, *Colloids Surf. A Physicochem. Eng. Asp.* **433**, 25 (2013)
33. D. Jiang, L. Chen, J. Xie, M. Chen, *Dalton Trans.* **43**, 4878 (2014)
34. J.P. Xiao, Y. Xie, R. Tang, W. Luo, *J. Mater. Chem.* **12**, 1148 (2002)
35. D. Ollis, P. Pichat, N. Serpone, *Appl. Catal. B* **99**, 377 (2010)
36. K.C. Christoforidis, A. Sengele, V. Keller, N. Keller, *A.C.S. Appl. Mater. Interfaces* **7**, 19324 (2015)
37. E.S. Elmolla, M. Chaudhuri, *Desalination* **252**, 46 (2010)